Evaluating the Quality of Ground-Based Microwave Radiometer Measurements and Retrievals Using Detrended Fluctuation and Spectral Analysis Methods

K. IVANOVA, E. E. CLOTHIAUX, AND H. N. SHIRER

Department of Meteorology, The Pennsylvania State University, University Park, Pennsylvania

T. P. ACKERMAN

Pacific Northwest National Laboratory, Richland, Washington

J. C. LILJEGREN

Environmental Research Division, Argonne National Laboratory, Argonne, Illinois

M. AUSLOOS

SUPRAS and GRASP, Institute of Physics, University of Liège, Liège, Belgium

(Manuscript received 15 March 2001, in final form 25 July 2001)

ABSTRACT

Time series both of microwave radiometer brightness temperature measurements at 23.8 and 31.4 GHz and of retrievals of water vapor and liquid water path from these brightness temperatures are evaluated using the detrended fluctuation analysis method. As quantified by the parameter α, this method (i) enables identification of the timescales over which noise dominates the time series and (ii) characterizes the temporal range of correlations in the time series. The more common spectral analysis method is also used to assess the data, and its results are compared with those from the detrended fluctuation analysis method. The assumption that measurements should have certain scaling properties allows the quality of the measurements to be characterized. The additional assumption that the scaling properties of the measurements of an atmospheric quantity are preserved in a useful retrieval provides a means for evaluating the retrieval itself. Applying these two assumptions to microwave radiometer measurements and retrievals demonstrates three points. First, the retrieved water vapor path during cloudy-sky periods can be dominated by noise on shorter-than-30-min timescales (α exponent = 0.1) and exhibits no scaling behavior at longer timescales. However, correlations in the brightness temperatures and liquid water path retrievals are found to be consistent with a power-law behavior for timescales up to 3 h with an α exponent equal to approximately 0.3, as in other geophysical phenomena. Second, clear-sky, *moist* atmospheres show the expected scaling for both measurements and retrievals of the water vapor path. Third, during clear-sky, *dry* atmospheric days, instrument noise from the 31.4-GHz channel compromises the quality of the water vapor path retrieval. The detrended fluctuation analysis method is thus proposed as means for assessing the quality of both the instrument data and the retrieved parameters obtained from these data.

1. Introduction

The U.S. Department of Energy (DOE) Atmospheric Radiation Measurement (ARM) Program (Stokes and Schwartz 1994) now operates two-channel microwave radiometers (Liljegren 1994) at its Southern Great Plains (SGP), Tropical Western Pacific (TWP), and North Slope of Alaska (NSA) sites. The DOE ARM microwave radiometers operate at frequencies of 23.8 and 31.4 GHz and are used to retrieve column water vapor and liquid water amounts (Liljegren and Lesht 1996). The range of atmospheric conditions across the three DOE ARM sites is extreme, raising questions concerning the reliability of the measurements and the retrievals. For these reasons, Liljegren (1999) has implemented an automated scheme for calibrating the instrument radiances at the different sites that dramatically improves their quality. Moreover, Liljegren et al. (2001) have developed a new retrieval for water vapor and liquid water path that attempts to remove biases resulting from changes in atmospheric conditions from one measurement to the next. Additional approaches to retrieving accurate estimates of column water vapor and liquid water paths currently are being pursued, such as the Bayesian approach adopted by McFarlane et al. (2000).

Corresponding author address: Kristinka Ivanova, Department of Meteorology, The Pennsylvania State University, 503 Walker Building, University Park, PA 16802.
E-mail: kristy@essc.psu.edu

An important motivation for the efforts of Liljegren et al. (2001) and McFarlane et al. (2000) is that the accuracy of the existing retrieval of cloud liquid water path (Westwater 1993; Liljegren and Lesht 1996) is not sufficient for many emerging studies on the interaction between stratus clouds and atmospheric radiation. In particular, biases over several-hour periods in the existing liquid water path retrieval frequently occur, rendering their use in atmospheric radiation transfer studies difficult at best. Using a specially designed analysis technique that is insensitive to these biases, we concentrate in this study on characterizing the quality of the measurements and retrievals based on assessment of the correlations between fluctuations in these signals. The emphasis here is on analyzing the fluctuations and ascertaining the temporal range over which they are correlated. This range is limited by the discretization step of the measurements and by the inherent lifetimes of cloudy or clear-sky atmospheric conditions.

Often the nonlinear processes at work in the atmosphere produce data series of such complexity that traditional statistical and spectral analyses techniques fail to extract meaningful physical information. Better techniques are clearly required. Recently, there have been several studies demonstrating that long-range power-law correlations (Peng et al. 1992) can be analyzed to give relevant timescales in, generally called, ''self-organized critical'' systems (Bak et al. 1989).

We study both the statistical properties of microwave radiometer measurements, as given by the 23.8- and 31.4-GHz channel brightness temperatures T_{B1} and T_{B2} and the liquid water path (LWP) and water vapor path (WVP) retrieved from them. As a means of assessing the validity of the retrievals, we determine how well they preserve the correlations of the fluctuations that initially exist in the measurements. We apply the ''detrended fluctuation analysis'' (DFA) method (Peng et al. 1994) to characterize the correlations in the signals. This method has been successfull in the investigation of long-range memory effects in biological (Stanley et al. 1993; Hausdorff et al. 1995) and financial (Vandewalle and Ausloos 1997; Ausloos and Ivanova 1999; Ausloos et al. 1999, 2000) data fluctuations, as well as to study long-range power-law correlations in the Southern Oscillation index (Ausloos and Ivanova 2001) and atmospheric signals to identify stratus cloud breaking (Ivanova and Ausloos 1999a; Ivanova et al. 2000).

We use the DFA to show that the water vapor path retrieval destroys the correlations in the brightness temperature measurements for a cloudy atmosphere and we propose an explanation for this (numerical) destruction. In addition, we characterize the contributions of instrument noise to the measurements during dry and moist clear-sky conditions.

Last, we contrast DFA method results to those from spectral analysis (Davis et al. 1994, 1996; Ivanova and Ackerman 1999) of the same signals, illustrating the strength of the DFA method relative to the spectral method for nonstationary conditions typifying the atmosphere.

The paper is organized as follows. In section 2 we describe the datasets and the retrieved quantities that are analyzed. Section 3 sketches the methods of analysis used, and the results are presented in section 4. The main findings of the study are discussed in section 5 and summarized in section 6, in which we also suggest directions for future work.

2. Data analyzed

The data used in this study are the radiances, recorded as brightness temperatures, measured with a Radiometrics, Inc., model WVR-1100 microwave radiometer at frequencies of 23.8 and 31.4 GHz and the vertical column amounts of cloud liquid water and water vapor retrieved from these measurements (Westwater 1993). The microwave radiometer is equipped with a Gaussian-lensed microwave antenna whose small-angle receiving cone is steered with a rotating flat mirror (information on microwave radiometers can be found online at http://www.arm.gov.) The data for this particular study are from the microwave radiometer located at the DOE ARM SGP central facility. For all four case study periods the microwave radiometer operated in vertically pointing mode. In this mode the radiometer makes sequential 1-s radiance measurements in each of the two channels while pointing vertically upward into the atmosphere. After collecting these radiances the radiometer mirror is rotated to view a blackbody reference target. For each of the two channels the radiometer records the radiance from the reference immediately followed by a measurement of a combined radiance from the reference and a calibrated noise diode. This measurement cycle is repeated once every 20 s.

A shorter measurement cycle does not necessarily lead to a larger number of independent samples. For example, clouds at 2 km of altitude moving at 10 m s^{-1} take 15 s to advect through a radiometer field-of-view of approximately 5°. Note that the 1-s sky radiance integration time ensures that the retrieved quantities correspond to a specific column of cloud above the instrument, as opposed to some longer time average of the cloud properties in the column above the instrument.

The field of view of the microwave radiometer is 5.7° at 23.8 GHz and 4.6° at 31.4 GHz. The brightness temperature is measured with a random error of approximately ± 0.5 K. The atmosphere is not optically thick at these two microwave radiometer frequencies during cloudy conditions. Hence, these two frequencies can be used to retrieve the total column amounts of water vapor and cloud liquid water. The error for the liquid water retrieval is estimated to be less than about 0.005 g cm^{-2} (Liljegren et al. 2001). The water vapor path retrievals are considered to have an absolute accuracy of better than 5%.

Three cases are considered in the current study: (i) a

6-day stratus-cloud event, 9–14 January 1998, which is an exceptionally long lasting cloudy period for the Southern Great Plains site that allows us to analyze an unusually long time series of 25 772 data points; (ii) a cloudless dry day, 29 September 1997, which has 3812 data points; and (iii) a cloudless moist day, 18 September 1997, which has 4296 data points.

3. Data analysis techniques

We use two techniques of analysis: the DFA and the more common technique of standard spectral analysis. The DFA technique (Peng et al. 1994) begins with dividing a random variable sequence $y(t)$ of length N into N/τ nonoverlapping boxes, each containing τ points. Then, the local trend (assumed to be linear in this investigation) $z(t) = at + b$ in each box is computed using a linear least squares fit to the data points in that box. It is worth noting that the trend assumption can be generalized without any difficulty (Vandewalle and Ausloos 1998) and without giving rise to drastic changes in the output results. This local trend removal should be contrasted to that of the common spectral analysis, in which the trend is sometimes removed over the entire time series.

We define the mean square difference over an interval of length τ as

$$F^2(\tau) = \frac{1}{\tau} \sum_{t=k\tau+1}^{(k+1)\tau} [y(t) - z(t)]^2, \qquad k = 0, 1, 2, \ldots, \left(\frac{N}{\tau} - 1\right). \quad (1)$$

Averaging $F^2(\tau)$ over the N/τ intervals gives the DFA function $\langle F^2(\tau)\rangle$ that describes the correlation in fluctuations as a function of τ. The procedure is repeated for almost all realistic τ-interval sizes, and the behavior of the DFA function is expected to follow a power law (Peng et al. 1994)

$$\langle F^2(\tau)\rangle^{1/2} \sim \tau^{\alpha}. \quad (2)$$

An exponent $\alpha \neq 1/2$ over a certain range of τ values implies the existence of long-range correlations in that time interval. In fact, the exponent α is equal to the Hurst exponent of the rescaled range (R/S) method, often denoted H_1, or H, in the literature (Hurst et al. 1965). An $\alpha < 1/2$ indicates antipersistence (Addison 1997), meaning that an increment in a signal is most likely followed by a decrement in the signal and vice versa. In contrast, $\alpha > 1/2$ indicates persistence whereby increments in a signal are most likely followed by additional increments, and decrements in a signal are most likely followed by additional decrements. For $\alpha = 0.5$, an increment in a signal is equally likely to be followed by either an increment or decrement and similarly for a decrement. Random Brownian motion signals are characterized by an exponent $\alpha = 0.5$, while Gaussian white noise sequences have $\alpha = 0$. For fractional Brownian motion, $\alpha \neq 0.5$ (Turcotte 1997; Addison 1997).

To relate the DFA results to more common analysis techniques, we investigate the high-frequency behavior of the fluctuations by applying the standard spectral analysis method (Panter 1965). The power spectral density $S(f)$ of an (assumed self-affine) time series $y(t)$ has a power-law dependence on frequency f,

$$S(f) \sim \frac{1}{f^{\beta}}, \quad (3)$$

following from the Fourier transform of the signal (Panter 1965). If the two scaling exponents α and β are well-defined, then the Wiener–Khinchin relation $\beta = 2\alpha + 1$ holds for $0 < \alpha < 1$ ($1 < \beta < 3$) (Turcotte 1997; Monin and Yaglom 1975; Heneghan and McDarby 2000). In terms of the exponents (α and β) of the signal, we can talk about pink noise $\alpha = 0$ ($\beta = 1$), brown noise $\alpha = 1/2$ ($\beta = 2$), or black noise $\alpha > 1/2$ ($\beta > 2$) (Schroeder 1991). Black noise is related to persistence. In contrast, inertial subrange turbulence for which $\beta = 5/3$ gives $\alpha = 1/3$ (Frisch 1995), which places it in the antipersistence regime.

The main advantages of the DFA method over other techniques, such as the Fourier transform (Panter 1965) and the rescaled range (Hurst et al. 1965) methods, are: (i) local and large-scale trends are avoided and (ii) the upper scaling limit (here the correlation time) crossover is well defined. In contrast, detrending of data before applying a Fourier transform leads to questions about the accuracy of the spectral exponent. For example, we know that the Fourier transform is inadequate for nonstationary signals. [An excellent discussion of these aspects may be found in Pelletier (1997).] Thus, we expect that the DFA method will allow a better understanding of the noise contribution to the retrieved sequences for different atmospheric conditions.

Last, in order to determine how a noise-like sequence alters the scaling properties of a signal, we also perform a sensitivity-to-noise study by adding synthetic Gaussian white noise with a mean of 0 and a variance of 1 to a signal with well-defined scaling properties. Namely, we added Gaussian white noise to the liquid water path signal for the cloudy-sky case period.

4. Results

We first present results from the cloudy-sky case study period to demonstrate the scaling properties expected of LWP retrievals (Ivanova et al. 2000; Davis et al. 1994). A similar analysis of WVP retrieval for the cloudy day yields different results. We next present results from the dry clear-sky case study to illustrate how the influence of instrument noise is characterized by the analysis technique and to determine the range of scales over which instrument noise dominates the statistics of

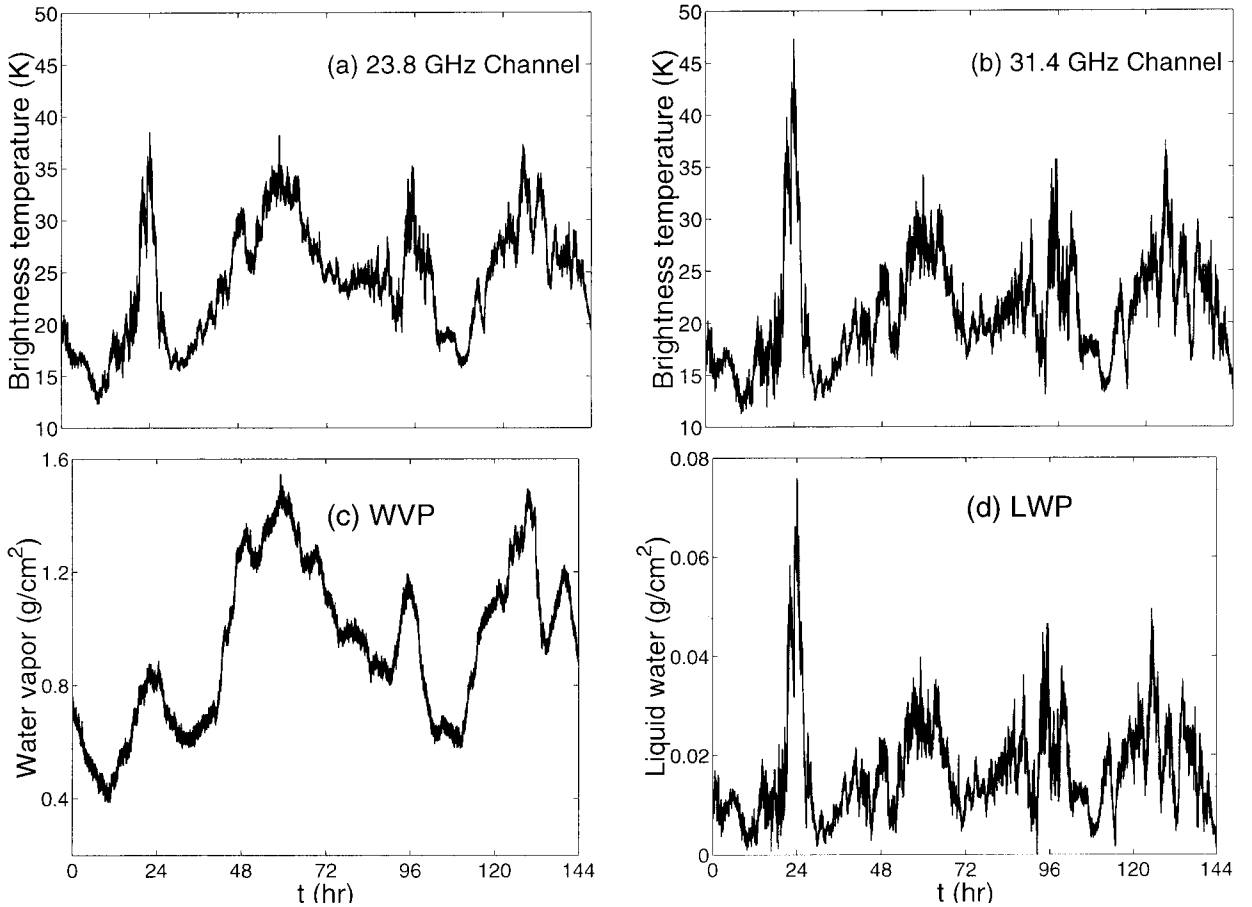

FIG. 1. Time dependence of the microwave radiometer (a) 23.8-GHz brightness temperature T_{B1}, (b) 31.4-GHz brightness temperature T_{B2}, (c) retrieved WVP, and (d) retrieved LWP for a cloudy case. These measurements were obtained at the ARM SGP site with time resolution of 20 s during the period from 9–14 Jan 1998. Each time series contains $N = 25\,772$ data points.

measured and retrieved quantities. The last case we consider is the moist clear-sky day.

a. Cloudy-sky atmosphere

Consider microwave radiometer brightness temperature measurements at 23.8 and 31.4 GHz, and retrieved liquid water path (LWP) and water vapor path (WVP) for a cloudy atmosphere. Data are plotted in Fig. 1. These measurements were obtained at the ARM Southern Great Plains site during the period from 9 to 14 January 1998 and consist of $N = 25\,772$ data points measured with a time resolution of 20 s. The DFA functions $\langle F^2(\tau)\rangle^{1/2}$ for the four time series are shown in Fig. 2. For this case the short-term fluctuation amplitudes in both the 23.8- and the 31.4-GHz frequency channels are clearly much larger than the 0.5 K fluctuations expected from instrument noise (see Figs. 1a,b). Hence, instrumental noise contribution is negligible and the brightness temperatures T_{B1} and T_{B2} for both the 23.8- and the 31.4-GHz frequency channels exhibit well-defined scaling properties from 3 to about 150 min with an exponent $\alpha = 0.36 \pm 0.01$ (see Figs. 2a,b and Table 1).

To estimate the correlations of the fluctuations in the liquid water retrieval we plot the DFA function in Fig. 2d for the LWP data shown in Fig. 1d. Part of this result has been presented in one of our previous studies (Ivanova et al. 2000). We view and discuss it here in the framework of both the direct radiance data T_{B1} and T_{B2} and the subsequent retrievals of liquid water path and water vapor path. Specifics of the retrieval method are discussed in section 5. Similar to the measured brightness temperatures T_{B1} and T_{B2}, the DFA function for the LWP follows a power law with an exponent $\alpha = 0.36 \pm 0.01$ holding over about two decades in time, that is, from 3 to 150 min. The correlation coefficient is $R = 0.997$. A crossover to Brownian-like motion with $\alpha = 0.47 \pm 0.03$ is readily seen for longer correlation times for T_{B1}, T_{B2} and LWP data in Figs. 2a,b,d.

One should note that the lower limit of the scaling range is determined by the resolution and discretization step of the measurements. Because a cloud moves at a

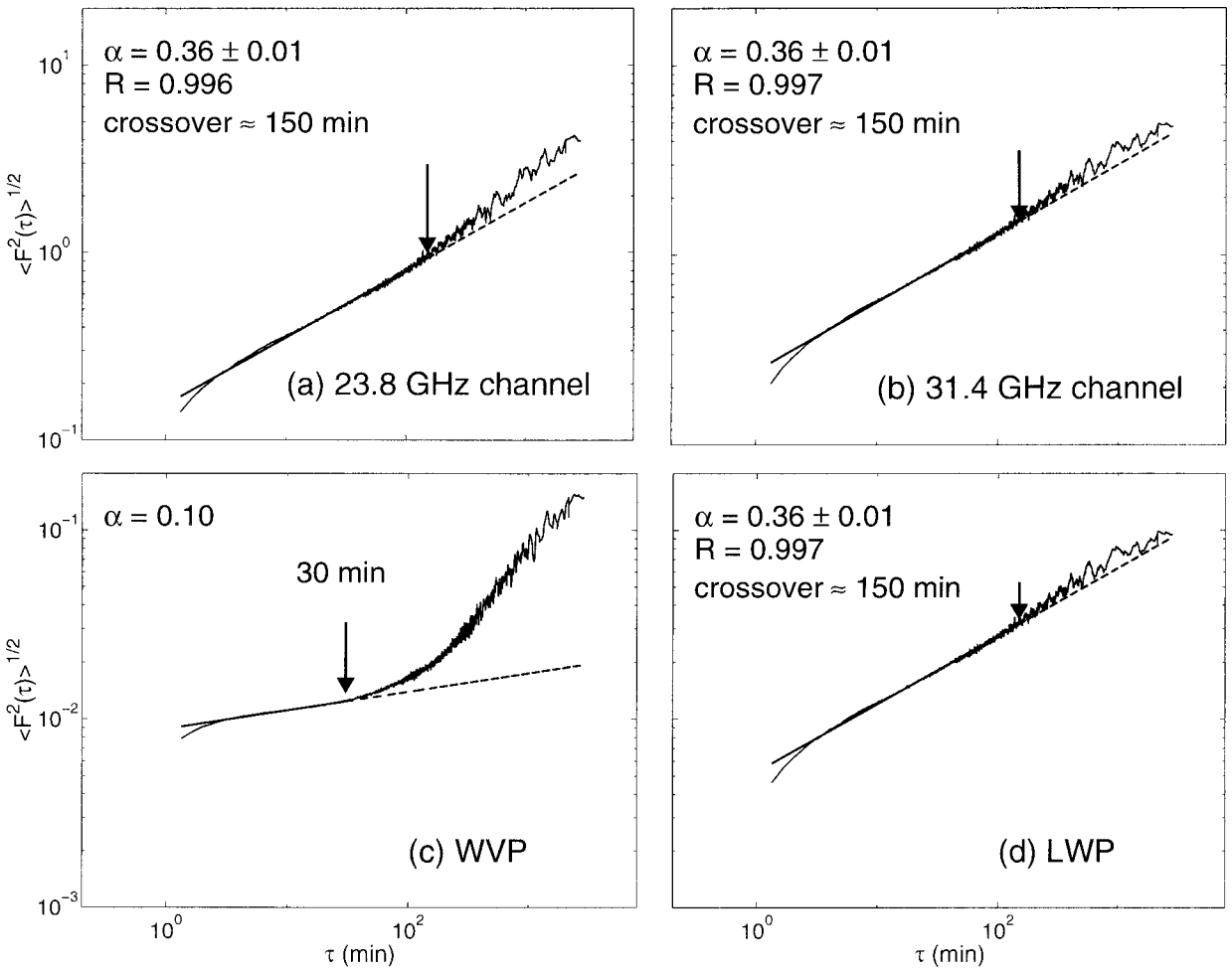

FIG. 2. The DFA function $\langle F^2(\tau)\rangle^{1/2}$ [Eq. (1)] for the data in Fig. 1. Well-defined scaling properties exist in cases (a), (b), and (d) for time ranges from about 5 to about 150 min. However, the WVP in (c) exhibits scaling for a very limited range; $\alpha = 0.1$ is obtained for the time range from about 3 to about 30 min.

typical speed of 10 m s^{-1} and the radiometer is always directed upward toward the same point in the atmosphere, the 20-s discretization step is chosen to ensure ergodic sampling over the 5° observation angle of the instrument. The upper scaling range limit depends on the lifetime of the cloud system. For the data in Fig. 1, the stratus cloud lasts for 6 days, which is an exceptionally long-lasting cloudy period for the Southern Great Plains site, allowing our access to an unusually long time series of 25 772 data points.

These results clearly support the hypothesis that power-law correlations exist in the fluctuations of the integrated cloud liquid water for a wide range of timescales. These power laws are interpreted as signatures of propagation of some *correlated information* across the cloud system for as long as 150 min. The results

TABLE 1. Values for the DFA α exponent [Eq. (1)] for the microwave radiometer measurements, 23.8- and 31.4-GHz channel brightness temperatures, and the retrieved LWP and WVP for the three cases considered in the text. Here, t_x denotes the upper scaling limit for which the α values are obtained. These α values can be compared with the β ones in Table 2 through the relationship $\beta = 2\alpha + 1$.

Case	t_x (min)	23.8 GHz	31.4 GHz	WVP	LWP
9–14 Jan 1998 (cloudy)	150	0.36 ± 0.01	0.36 ± 0.01	(0.10) (t_x = 30 min)	0.36 ± 0.01
29 Sep 1997 (cloudless, dry)	150	0.21 ± 0.01	0.10 ± 0.007	0.19 ± 0.01	0.06 ± 0.007
18 Sep 1997 (cloudless, moist)	240	0.33 ± 0.02	0.23 ± 0.02	0.31 ± 0.02	0.07 ± 0.009

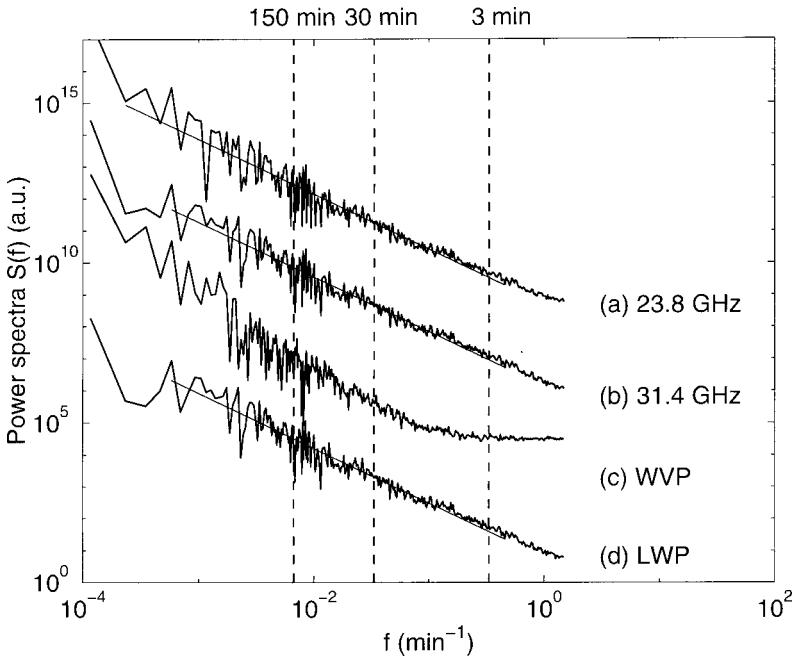

FIG. 3. Power spectra $S(f)$ for the data in Fig. 1. Note the consistency in (a), (b), and (d), but the WVP spectrum (c) becomes noisy at high frequencies. For clarity, the spectra are offset along the ordinate.

for the liquid water path and the two brightness temperature measurements are also consistent with the calculation of the first-order $H_q|_{q=1}$ exponent; here, $H_1 = 0.29$ as obtained from a separate multifractal analysis (Marshak et al. 1997; Ivanova and Ausloos 1999b; Kiely and Ivanova 1999; Tessier et al. 1993; Lovejoy et al. 1996) of remotely measured liquid water path (Ivanova and Ackerman 1999) and of directly measured liquid water content in an oceanic stratus-cloud system (Davis et al. 1994).

In contrast, the scaling properties of the retrieved water vapor path are compromised. The DFA-function (plotted in Fig. 2c) exhibits noiselike fluctuations from about 3 to about 30 min with an exponent $\alpha \approx 0.10$ (Table 1). To understand the reason for this behavior in the water vapor column retrieval for a cloudy atmosphere we examine in section 5 each step of the retrieval procedure to determine where the change in the correlations of the fluctuations occurs (Westwater 1978; Liljegren and Lesht 1996).

We relate the DFA results to those given by a spectral analysis of the brightness temperatures T_{B1} and T_{B2} and the two retrievals, whose spectra are plotted in Fig. 3. The scaling properties of the LWP and the two brightness temperatures are characterized by exponents β that are consistent, within large error bars, with the DFA-α values according to the relation $\beta = 2\alpha + 1$ (Table 2). The WVP spectrum (Fig. 3c) exhibits a noiselike contribution at high frequencies that corresponds to the short timescales given by the DFA function in Fig. 2c. The large variability in the power spectra leads to large uncertainties in the estimates of the spectral (β) exponent. This problem of the discrete Fourier transform is known as spectral variance and has been discussed comprehensively by many authors, among them Priestly (1981) and Percival and Walden (1994).

TABLE 2. Values of the spectral exponent β [Eq. (3)] for the microwave radiometer measurements, 23.8- and 31.4-GHz channel brightness temperatures, and the retrieved LWP and WVP for the three cases considered in the text. Values of β exponents are obtained for (i) within time interval of [3, 1718] min (Fig. 3); for (ii) within time interval of [2, 100] min (Fig. 6); and for (iii) within time interval of [2, 110] min (Fig. 10). The β values for the WVP in the (i) and LWP in the (ii) and (iii) cases cannot be properly estimated.

Case	N_{data}	23.8 GHz	31.4 GHz	WVP	LWP
9–14 Jan 1998 [(i) cloudy]	25 772	1.72 ± 0.04	1.71 ± 0.04		1.72 ± 0.04
29 Sep 1997 [(ii) cloudless, dry]	3812	1.48 ± 0.06	0.87 ± 0.06	1.48 ± 0.06	
18 Sep 1997 [(iii) cloudless, moist]	4296	1.70 ± 0.07	1.55 ± 0.05	1.66 ± 0.06	

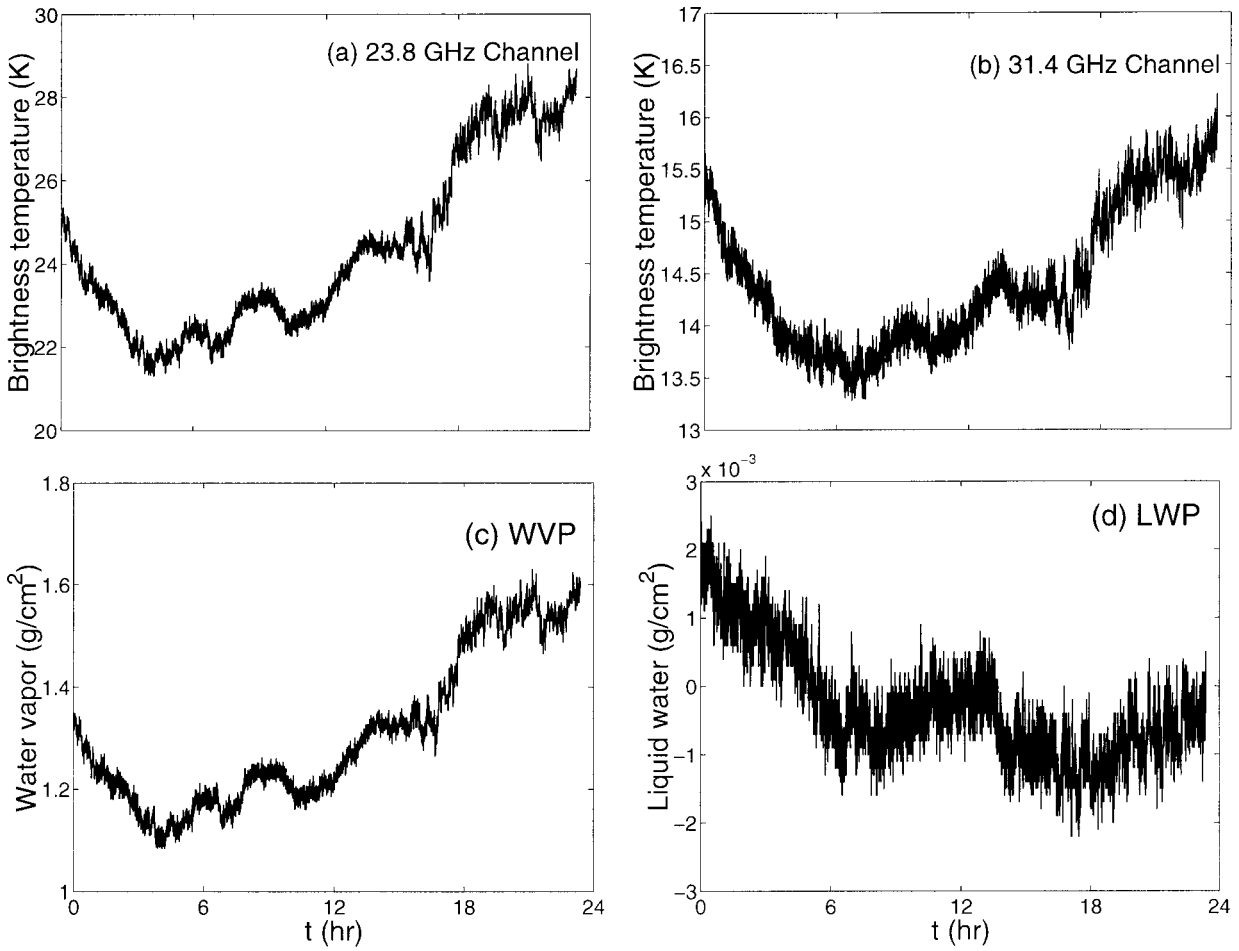

FIG. 4. Time dependence of the microwave radiometer (a) 23.8-GHz brightness temperature T_{B1}, (b) 31.4-GHz brightness temperature T_{B2}, (c) retrieved WVP, and (d) retrieved LWP for a dry cloudless case. These measurements were obtained at the ARM SGP site on 29 Sep 1997. Each time series contains $N = 3812$ data points with a time resolution of 20 s.

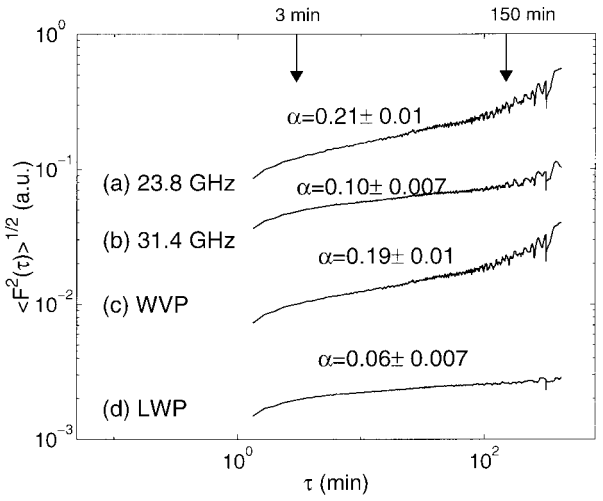

FIG. 5. The DFA function $\langle F^2(\tau)\rangle^{1/2}$ for the data in Fig. 4. The DFA functions in (b) illustrate that the 31.4-GHz brightness temperature channel is dominated by instrumental noise due to the very low levels of absolute humidity. The total precipitable water is on the order of 0.9 cm.

b. Dry clear-sky atmosphere

To test whether the correlations of the fluctuations are preserved for other atmospheric conditions, we analyze the brightness temperature measurements T_{B1} and T_{B2} and the retrieved liquid water path and water vapor path for an extremely dry clear sky (Fig. 4). The precipitable water estimated by radiosonde measurements for this dry day, 29 September 1997, is on the order of 0.9 cm. These measurements were obtained at the ARM Southern Great Plains site and consist of $N = 3812$ data points measured with a time resolution of 20 s.

The DFA functions $\langle F^2(\tau)\rangle^{1/2}$ for these four data series are shown in Fig. 5. The DFA function in Fig. 5b illustrates that the 31.4-GHz brightness temperature channel is dominated by instrumental noise at short timescales as a result of both the very low levels of absolute humidity and the absence of any liquid water. As expected, the influence of instrument noise on the 31.4-GHz channel is particularly severe. The spectral analysis result (Fig. 6) can be interpreted along these lines as

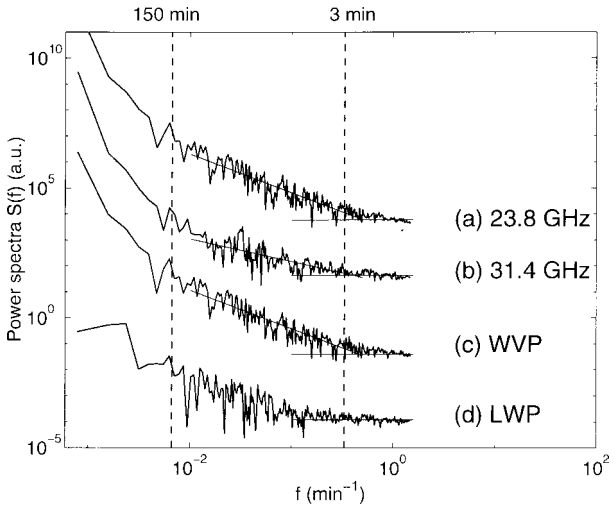

FIG. 6. Power spectra $S(f)$ for the data in Fig. 4. The (b) 31.4-GHz channel and (d) LWP spectra suggest that the brightness temperature records and LWP retrieval at high frequencies for a dry cloudless atmosphere are dominated by the microwave radiometer instrumental noise.

well. The drop in the value of α from the measured to the retrieved quantities (Fig. 5, Table 1) for the time range from about 3 to 150 min is a result of adding measurement noise in the retrieval process (section 5). For this dry clear-sky case the LWP signal analysis demonstrates noise in the LWP over all timescales, which is expected owing to the absence of cloud liquid water. The retrieval of small LWP values in the absence of actual cloud liquid water is an artifact of the retrieval process. This problem is being addressed with an improved retrieval algorithm (Liljegren et al. 2001; McFarlane et al. 2000).

To determine how a noiselike sequence alters the scaling properties of a signal with well-defined scaling properties when it is superimposed on a signal, we performed an idealized sensitivity-to-noise study. We add a synthetic Gaussian white noise with a mean of 0 and a variance of 1 to the liquid water path data in Fig. 1d. The original signal is anticorrelated with $\alpha = 0.36$. The noise signal is added in successive steps with an amplitude ϵ ranging from 1/16 to 1/2 of the LWP signal amplitude. Results for the DFA function $\langle F^2(\tau)\rangle^{1/2}$ for two cases, 1/4 and 1/2 noise-to-signal ratio, are plotted in Fig. 7a as curves (ii) and (iii). The α values for the noisy signals are plotted in Fig. 7b as a function of the noise-to-signal ratio ϵ, which can be viewed as representing the degree of noise contamination. An exponential decrease of the α values relative to zero-noise-value $\alpha = 0.36$, where ϵ is observed for the LWP signal.

In Fig. 7c the respective power spectra are plotted. Note that spectrum labeled (iii) in Fig. 7c, which is the spectrum of a complex signal obtained from the superposition of Gaussian white noise on the LWP signal, is very similar to the spectrum of the WVP retrieval shown in Fig. 3c. However, the DFA function labeled (iii) in

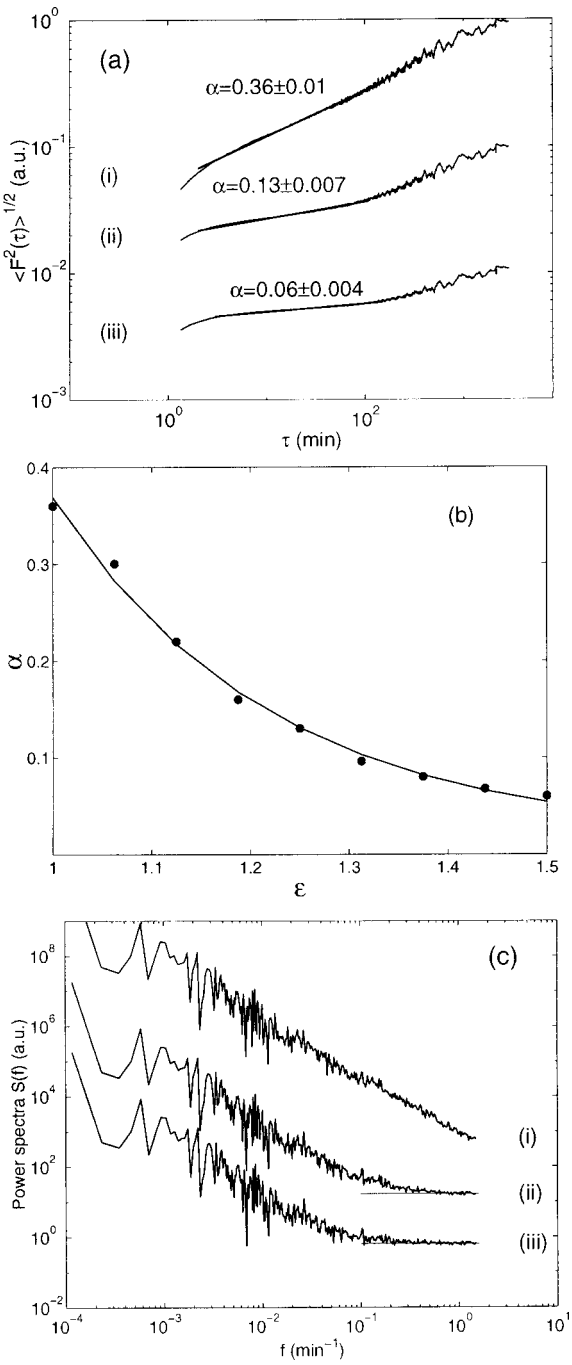

FIG. 7. (a) DFA function $\langle F^2(\tau)\rangle^{1/2}$ for the LWP data illustrated in Fig. 1d is labeled (i). Adding Gaussian white noise with amplitude of 1/4 and 1/2 of the LWP signal amplitude to the LWP signal results in the DFA fluctuation function $\langle F^2(\tau)\rangle^{1/2}$ labeled (ii) and (iii), respectively. (b) The α exponent for the LWP signal (in Fig. 1d) with added Gaussian white noise as a function of the noise-to-signal ratio ϵ. The beginning of the abscissa corresponds to the LWP signal without noise ($\epsilon = 1$). Exponential decay is found to be the best fit, showing that adding noise to a noisy signal produces an extremely small effect. (c) Power spectra for the three cases shown in (a), in which the effects of the noise are clearly seen at high frequencies.

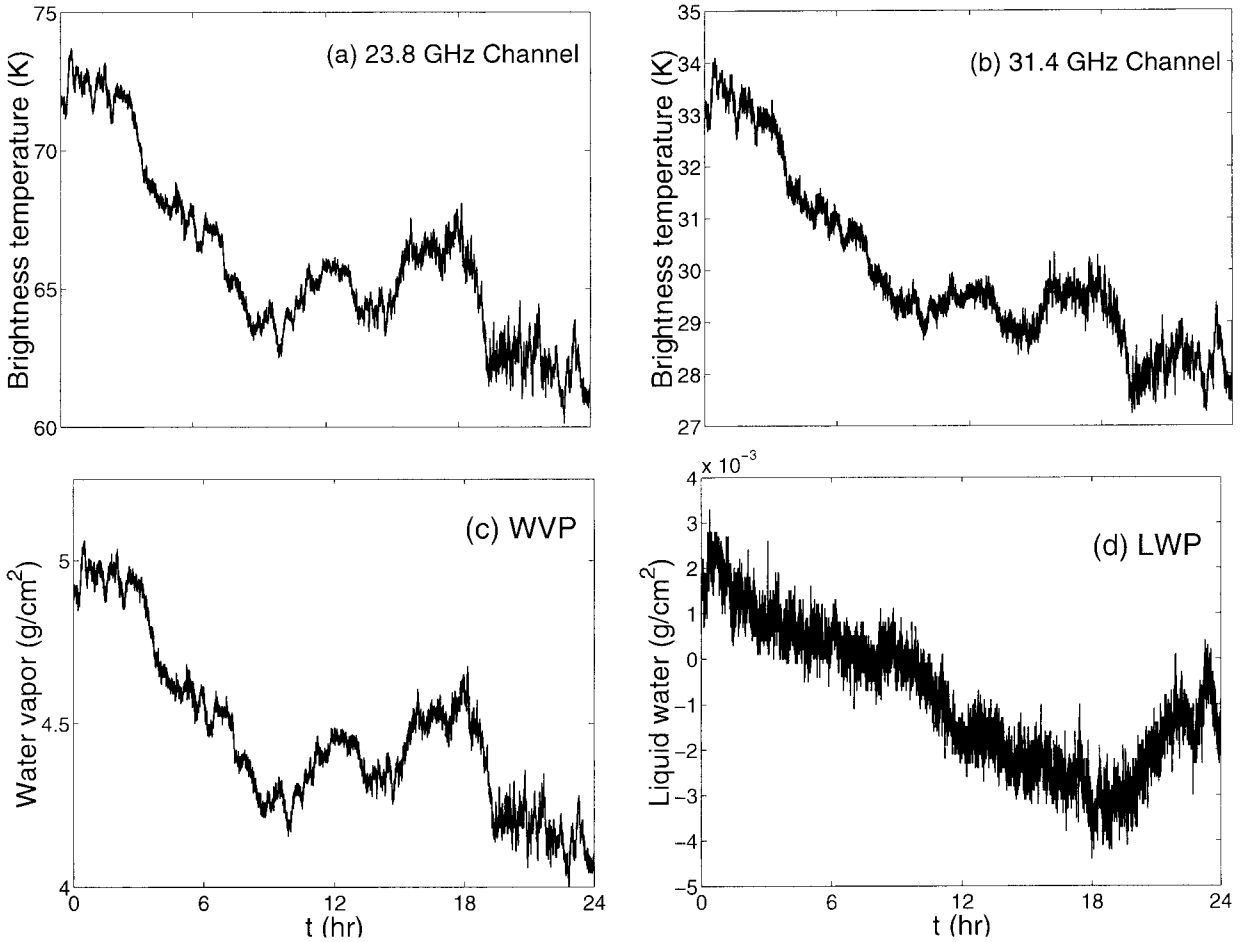

FIG. 8. Time dependence of the microwave radiometer (a) 23.8-GHz brightness temperature T_{B1}, (b) 31.4-GHz brightness temperature T_{B2}, (c) retrieved WVP, and (d) retrieved LWP for a moist cloudless case. These measurements were obtained at the ARM SGP site on 18 Sep 1997. Each time series contains $N = 4296$ data points with a time resolution of 20 s.

Fig. 7a of the same complex signal is similar to the DFA function in Fig. 2c at small timescales only. The differences at large timescales are related to the fact that the data series analyzed are different, one being the LWP signal plus white noise and the other being the WVP retrieval data (Fig. 1c). Spectral analysis shows noise in both cases, whereas the detrended fluctuation analysis method finds differences between the two time series, which emphasize some of the advantages of the detrended fluctuation analysis over the spectral analysis method when studying correlations and anticorrelations of the fluctuations of a signal.

c. Moist clear-sky atmosphere

The day 18 September 1997 is an example of a cloudless day that has a very high level of absolute humidity. The precipitable water on this day is on the order of 4–5 cm. Data consist of $N = 4296$ data points and are plotted in Fig. 8 for the microwave radiometer brightness temperatures T_{B1} and T_{B2} and the two retrievals. The measured brightness temperatures in both channels have values that are substantially greater than the cosmic background plus instrument noise (Figs. 8a,b). Detrended fluctuation analysis of the measurements and retrievals highlight this aspect of the data (Fig. 9). The 23.8-GHz brightness temperature measurements and the retrieved WVP scale with exponents $\alpha = 0.33 \pm 0.02$ and $\alpha = 0.31 \pm 0.02$ over approximately a 4-h interval (Table 1). However, the 31.4-GHz brightness temperature measurements scale with an exponent of $\alpha = 0.23 \pm 0.02$, exhibiting a higher degree of anticorrelation in the fluctuations as found when there are relatively higher noise contributions (Fig. 7b). This result is not unexpected, because the 31.4-GHz channel is more sensitive to cloud liquid water.

The spectral analysis results are plotted in Fig. 10. Spectral scaling exponents β estimated for the frequency range consistent with the lower-scale range of the DFA function for the two brightness temperature measurements and the WVP retrieval. They are summarized in Table 2. Each β exponent is found to be in agreement

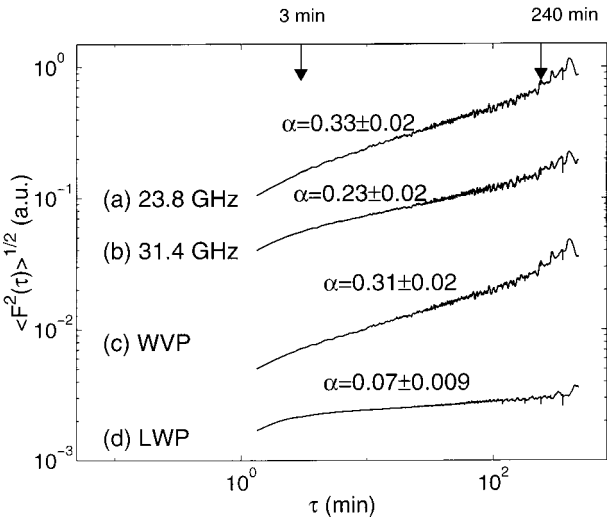

FIG. 9. The DFA function $\langle F^2(\tau)\rangle^{1/2}$ for the data in Fig. 8. The DFA function in (d) illustrates that the retrieved LWP is a noiselike sequence. This is an expected result for a cloudless, moist atmosphere. The total precipitable water is on the order of 2.5 cm.

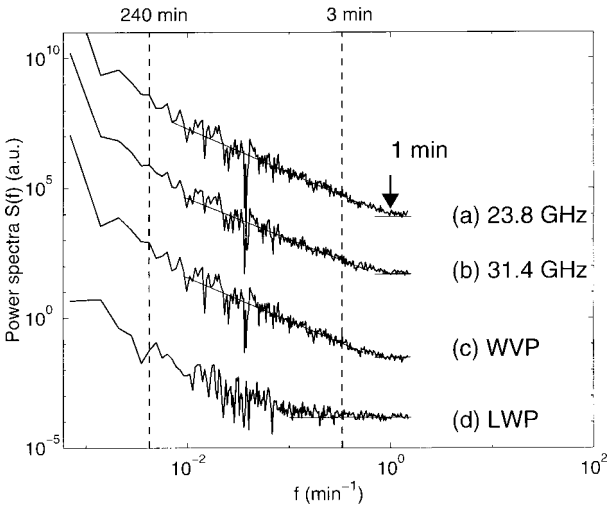

FIG. 10. Power spectra $S(f)$ for the case of cloudless, moist atmosphere (data in Fig. 8). Both 23.8 and 31.4-GHz channels spectra, as well as the water path retrieval, show noiselike scaling below 1 min.

within the error bars with the corresponding α value for the same data via the theoretical relation $\beta = 2\alpha + 1$ (Table 1). The flat, high-frequency parts of the spectra in Fig. 10 for periods below 1 min illustrate the contribution of noise even to measurements and retrievals under moist, clear-sky atmospheric conditions. The very high frequency noise for time periods below 1 min is better identified by the spectral analysis than by the DFA method.

5. Discussion

The loss of scaling in the WVP retrievals for the cloudy-sky case study period was not anticipated and requires an explanation. We now briefly outline the WVP and LWP retrieval scheme (Westwater 1978; Liljegren and Lesht 1996) in order to identify the step in the retrieval at which noiselike behavior is introduced into the WVP retrieval.

If the total atmospheric transmission at frequency ν is written as $\exp(-\tau_\nu)$, then measurements of microwave radiometer brightness temperature $T_{B\nu}$ can be converted to opacity τ_ν by

$$\tau_\nu = \ln\left[\frac{(T_{mr} - T_c)}{(T_{mr} - T_{B\nu})}\right], \tag{4a}$$

where T_c is the cosmic background ''big-bang'' brightness temperature equal to 2.8 K and T_{mr} is an estimated ''mean radiating temperature'' of the atmosphere. [Note that Eq. (4a) holds for nonprecipitating clouds, i.e., clouds having drops sufficiently small that scattering is negligible.] Writing τ_ν in terms of atmospheric constituents, we have

$$\tau_\nu = \kappa_{V\nu} V + \kappa_{L\nu} L + \tau_{d\nu}, \tag{4b}$$

where $\kappa_{V\nu}$ and $\kappa_{L\nu}$ are path-averaged mass absorption coefficients of water vapor and liquid water and $\tau_{d\nu}$ is the absorption by dry atmosphere constituents (i.e., oxygen). Removing the dry atmosphere opacity from τ_ν, we have

$$\tau_\nu^* = \tau_\nu - \tau_{d\nu} = \ln\left[\frac{(T_{mr} - T_c)}{(T_{mr} - T_{B\nu})}\right] - \tau_{d\nu}. \tag{5}$$

From measurements at the 23.8-GHz channel, sensitive primarily to water vapor, and the 31.4-GHz channel, sensitive primarily to cloud liquid water, we can write two equations for the opacity at the two frequencies and solve them for the two unknowns L and V:

$$L = l_1 \tau_{\nu_1}^* + l_2 \tau_{\nu_2}^* \quad \text{(LWP), and} \tag{6}$$

$$V = v_1 \tau_{\nu_1}^* + v_2 \tau_{\nu_2}^* \quad \text{(WVP),} \tag{7}$$

where

$$l_1 = -\left(\kappa_{L\nu_2}\frac{\kappa_{V\nu_1}}{\kappa_{V\nu_2}} - \kappa_{L\nu_1}\right)^{-1},$$

$$l_2 = \left(\kappa_{L\nu_2} - \kappa_{L\nu_1}\frac{\kappa_{V\nu_2}}{\kappa_{V\nu_1}}\right)^{-1},$$

$$v_1 = \left(\kappa_{V\nu_1} - \kappa_{V\nu_2}\frac{\kappa_{L\nu_1}}{\kappa_{L\nu_2}}\right)^{-1}, \quad \text{and}$$

$$v_2 = \left(\kappa_{V\nu_1}\frac{\kappa_{L\nu_2}}{\kappa_{L\nu_1}} - \kappa_{V\nu_2}\right)^{-1}. \tag{8}$$

To identify the retrieval step that produces changes in the correlations of the fluctuations, we perform DFA analysis on time series of

$$(T_{mr} - T_c)/(T_{mr} - T_{B\nu}) \tag{9}$$

TABLE 3. Datasets used to trace the changes in the correlations analysis.

23-GHz ratio using monthly averaged mean radiating temperature
31-GHz ratio with monthly averaged mean radiating temperature
23-GHz optical path using monthly averaged mean radiating temperature
31-GHz optical path using monthly averaged mean radiating temperature
Water vapor path using monthly averaged mean radiating temperature
Liquid water path using monthly averaged mean radiating temperature
23-GHz ratio using instantaneous estimated mean radiating temperature
31-GHz ratio with instantaneous estimated mean radiating temperature
23-GHz optical path using instantaneous estimated mean radiating temperature
31-GHz optical path using instantaneous estimated mean radiating temperature
Water vapor path using instantaneous estimated mean radiating temperature
Liquid water path using instantaneous estimated mean radiating temperature
Water vapor path (variable coefficients)
Liquid water path (variable coefficients)

and Eqs. (5), (6), and (7) for the cloudy-sky case study period. To understand whether holding T_{mr} constant in Eqs. (5), (6), and (7) is the source of the noise, we generate two time series from each of Eqs. (5), (6), and (7) (Table 3). In the first time series for each equation we hold T_{mr} fixed at its monthly averaged climatological value (Table 4), as in the retrieval, while for each of the second time series we estimate a new value of T_{mr} for each 20-s sample using other measurements available at the DOE ARM SGP site. We do this for each of the two frequencies ν, generating a total of 12 sequences. In these 12 sequences we kept the absorption coefficients $\kappa_{L\nu}$ and $\kappa_{V\nu}(\nu = \nu_1, \nu_2)$ fixed. The new scheme of Liljegren et al. (2001) allows for variable absorption coefficients and mean radiating temperatures in the retrieval of WVP and LWP. So, we implement their new scheme and perform a WVP and LWP retrieval with it for this cloudy-sky case study period. Overall, we generated 14 time series to which we apply the DFA analysis.

For all 14 data sequences, except the three water vapor signals, the DFA functions scale with exponent $\alpha = 0.36 \pm 0.01$, as did the original measurements of both T_{B1} and T_{B2}. In contrast, each of the three water vapor path data sequences has the same noiselike, short-range scaling behavior. Therefore, the change in short-term fluctuations of retrieved water vapor path does not result from fixed coefficients and mean radiating temperatures, but rather from the transformation of the signals from opacity [Eq. (5)] to WVP [Eq. (7)]. Although the transformation from brightness temperature to opacity [Eq. (5)] involves a nonlinear operation, we find that the logarithmic operation preserves the character of the fluctuations.

TABLE 4. Monthly climatological values of the retrieval coefficients, l_1, l_2, and v_1, v_2 in Eq. (6), showing that $r_l = l_2/l_1 \approx -3.5$ and $r_v = v_1/v_2 \approx -2$.

Month	l_1	l_2	v_1	v_2
Jan	−0.144 389	0.567 176	21.6227	−12.6037
Feb	−0.153 517	0.554 340	21.1463	−12.4573
Mar	−0.188 830	0.653 695	22.1970	−12.9066
Apr	−0.258 638	0.776 852	22.2173	−12.6780
May	−0.308 970	0.878 312	22.7005	−12.8789
Jun	−0.290 936	0.823 459	22.4033	−11.5986
Jul	−0.247 642	0.751 842	22.8299	−13.2155
Aug	−0.268 197	0.803 732	23.1813	−13.4728
Sep	−0.261 245	0.774 673	22.7105	−13.2431
Oct	−0.234 130	0.731 487	22.8530	−13.2600
Nov	−0.224 780	0.722 879	22.0715	−12.7427
Dec	−0.143 773	0.623 870	21.7302	−12.5548

To understand why Eqs. (6) and (7), which are similar, exhibit different scaling properties, we analyze the relative magnitudes and signs of l_1, l_2, v_1, and v_2 in conjunction with the range and fluctuations in the brightness temperature measurements T_{B1} and T_{B2}. Atmospheric brightness temperatures and opacities, as well as their fluctuations, at the frequencies of the two channels depend on the emission of water vapor, liquid water (for a cloudy atmosphere), and molecular oxygen (Fig. 11). As Fig. 11 illustrates, the 31.4-GHz channel is more sensitive than the 23.8-GHz channel to variations in liquid water path. In fact, for the cloudy sky the 31.4-GHz brightness temperatures T_{B2} fluctuate with amplitudes about 2 times as large as the amplitudes of the 23.8-GHz brightness temperatures T_{B1}:

$$\delta T_{B1} \approx \frac{1}{2}\delta T_{B2}, \tag{10a}$$

and from Eqs. (4) and (5) we have

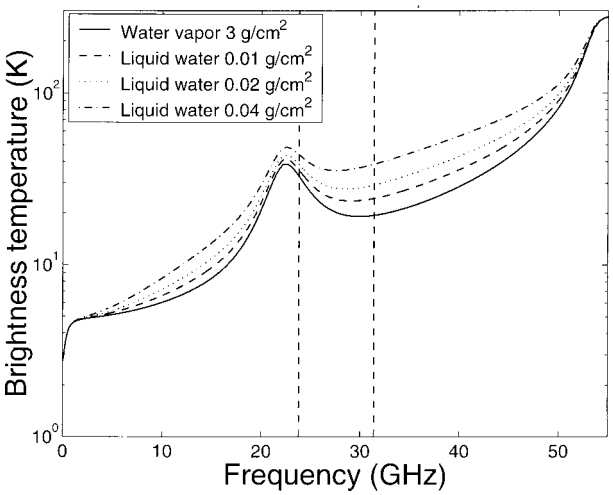

FIG. 11. Microwave radiometer emission spectra computed with the code of Schroeder and Westwater (1991). The solid curve corresponds to the spectrum of water vapor, and the other curves represent the spectra for different amounts of liquid water in the atmosphere.

$$\delta\tau^*_{\nu 1} \approx \frac{1}{2}\delta\tau^*_{\nu 2}. \quad (10b)$$

Inspection of the WVP retrieval coefficients in Table 4 shows that

$$v_1 \approx -2v_2. \quad (10c)$$

Inspecting Eq. 10 in the context of Eq. (7), we see that the contributions of the fluctuations in the two channels to WVP are approximately equal in magnitude but opposite in sign and lead to a numerical phenomenon known as catastrophic cancellation (Blum 1972). Therefore, the small-scale fluctuations in the WVP sequences during the cloudy-sky period appear as noise in the DFA function and at high frequencies in the power spectrum.

During the cloudy-sky period, a comparable problem does not occur in the LWP retrieval. For the LWP retrieval

$$l_1 \approx -l_2/3.5, \quad (10d)$$

and the 31.4-GHz channel term in Eq. (6) is dominant, preventing catastrophic cancellation as in Eq. (7) for the cloudy-sky period.

The relative magnitudes between the two terms in Eqs. (6) and (7), and the influence of instrument noise on them, also explain the dry and moist clear-sky results. For a cloud-free sky, as the column moisture increases, the ratio of the 23.8- to 31.4-GHz brightness temperature increases (e.g., cf. Figs. 4 and 8), just the opposite to what happens on a cloudy-sky day with increasing column liquid (Fig. 11). Consequently, for clear-sky periods the second term of Eq. (7) becomes increasingly important.

For clear-sky dry periods (section 4b), the small-scale fluctuations of the 31.4-GHz signal are dominated by instrument noise, because the amplitude levels are below the threshold for sensitivity to vapor at that frequency, as seen from the microwave radiometer spectrum (Fig. 11). Therefore, the WVP retrieval algorithm expressed by Eq. (7) becomes noisier.

For a clear-sky moist atmosphere (section 4c), since the ratio of the 23.8- to 31.4-GHz brightness temperature is markedly different than 1, Eq. (10c) does not have such an impact on Eq. (7), the WVP retrieval algorithm, as it does for cloudy-sky periods.

The LWP retrieval during clear-sky periods is always dominated by noise since the second term in Eq. (6) is always significant.

6. Summary

Time series of both microwave radiometer brightness temperature measurements at 23.8 and 31.4 GHz and retrievals of water vapor and liquid water path from the brightness temperatures are evaluated using both the detrended fluctuation analysis method and the spectral analysis method. We show that the detrended fluctuation analysis method is useful for analyzing the power-law correlations in such atmospheric signals. In particular, the present analysis demonstrated the validity of the liquid water path retrieval for a cloudy-sky day and the water vapor path retrieval for a clear-sky moist day.

We found the water vapor path signal to be dominated by noise for a cloudy atmosphere on timescales less than 30 min. The appearance of noiselike correlations arises from the specific relationships between the coefficients in the water vapor retrieval equation, the magnitudes of both the measurements, and fluctuations in the brightness temperature measurements. The latter leads to catastrophic cancellation of two terms of a similar amplitude and opposite sign and is related to the sensitivity of the measurements to liquid water content at these frequencies.

On both clear-sky days, instrument noise is readily apparent in the 31.4-GHz channel measurements owing to the absence of emission from liquid water. In the water vapor path retrieval, noise in the 31.4-GHz channel measurements blurs correlations present in the vapor-sensitive channel measurements. For a clear-sky dry atmosphere, instrument noise is readily apparent in the 31.4-GHz channel measurements owing to the absence of liquid water. This noise artificially blurs the correlations existing in the vapor-sensitive channel when the WVP retrieval is performed.

Since November 1996, the DOE ARM Program has been collecting coincident microwave radiometer and millimeter-wave cloud radar data at its SGP site. We will use detrended fluctuation analysis and spectral analysis methods, together with other approaches from statistical physics, to analyze the temporal properties of boundary layer clouds that have occurred since November 1996. The aim of this next step will be to classify boundary layer clouds according to their statistical properties and to relate these properties to the underlying dynamics of the cloud fields. This step will lead to better understanding of the impact of different cloud types on the radiation field.

Acknowledgments. This research was supported in part by the Department of Energy through Grant Battelle 327421-A-N4; the Department of Energy through Grant DE-FG02-90ER61071; and in part by the U.S. Department of Energy, Office of Science, Office of Biological and Environmental Research, Environmental Sciences Division, under Contract W-31-109-Eng-38, as part of the Atmospheric Radiation Measurement Program. We thank Ed Westwater and Roger Marchand for stimulating discussions.

REFERENCES

Addison, P. S., 1997: *Fractals and Chaos: An Illustrated Course.* Institute of Physics, 250 pp.

Ausloos, M., and K. Ivanova, 1999: Precise (m, k)-Zipf diagram analysis of mathematical and financial time series when $m = 6$ and $k = 2$. *Physica A,* **270,** 526–542.

——, and ——, 2001: Power law correlations in the Southern Os-

cillation index fluctuations characterizing El Niño. *Phys. Rev. E,* **64,** 047201.
——, N. Vandewalle, Ph. Boveroux, A. Minguet, and K. Ivanova, 1999: Applications of statistical physics to economic and financial topics. *Physica A,* **274,** 229–240.
——, ——, and K. Ivanova, 2000: Time is money. *Noise, Oscillators and Algebraic Randomness,* M. Planat, Ed., Noise in Communication Systems to Number Theory, Vol. 550, Springer, 156–171.
Bak, P., K. Chen, and M. Creutz, 1989: Self-organized criticality in the ''game of life.'' *Nature,* **342,** 780–783.
Blum, E. K., 1972: *Numerical Analysis and Computation Theory and Practice.* Addison-Wesley, 612 pp.
Davis, A., A. Marshak, W. Wiscombe, and R. Cahalan, 1994: Multifractal characterization of nonstationarity and intermittency in geophysical fields: Observed, retrieved or simulated. *J. Geophys. Res.,* **99** (D4), 8055–8072.
——, ——, ——, and ——, 1996: Scale invariance in liquid water distributions in marine stratocumulus. Part I: Spectral properties and stationary issues. *J. Atmos. Sci.,* **53,** 1538–1558.
Frisch, U., and A. N. Kolmogorov, 1995: *Turbulence: The Legacy of A. N. Kolmogorov.* Cambridge University Press, 296 pp.
Hausdorff, J. M., C.-K. Peng, Z. Ladin, J. Y. Wei, and A. L. Goldberger, 1995: Is walking a random walk? Evidence for long-range correlations in the stride interval of human gait. *J. Appl. Physiol.,* **78,** 349–358.
Heneghan, C., and G. McDarby, 2000: Establishing the relation between detrended fluctuations analysis and power spectral density analysis for stochastic processes. *Phys. Rev. E,* **62,** 6103–6110.
Hurst, H. E., B. P. Black, and Y. M. Simaika, 1965: *Long-Term storage: An Experimental Study.* Constable.
Ivanova, K., and T. Ackerman, 1999: Multifractal characterization of liquid water in clouds. *Phys. Rev. E,* **59,** 2778–2782.
——, and M. Ausloos, 1999a: Application of the Detrended Fluctuation Analysis (DFA) method for describing cloud breaking. *Physica A,* **274,** 349–354.
——, and ——, 1999b: Low q-moment multifractal analysis of gold price, Dow Jones Industrial Average and BGL-USD exchange rate. *Eur. Phys. J. B,* **8,** 665–669.
——, ——, E. E. Clothiaux, and T. P. Ackerman, 2000: Break-up of stratus cloud structure predicted from non-Brownian motion liquid water and brightness temperature fluctuations. *Europhys. Lett.,* **52,** 40–46.
Kiely, G., and K. Ivanova, 1999: Multifractal analysis of hourly precipitation. *Phys. Chem. Earth,* **24** 781–786.
Liljegren, J. C., 1994: Two-channel microwave radiometer for observations of total column precipitable water vapor and cloud liquid water path. Preprints, *Fifth Symp. on Global Change Studies,* Nashville, TN, Amer. Meteor. Soc., 262–269.
——, 1999: Automatic self-calibration of ARM microwave radiometers. *Microwave Radiometry and Remote Sensing of the Earth's Surface and Atmosphere,* P. Pampaloni and S. Paloscia, Eds., VSP Press, 433–443.
——, and B. M. Lesht, 1996: Measurements of integrated water vapor and cloud liquid water from microwave radiometers at the DOE ARM cloud and radiation testbed in the U.S. Southern Great Plains. *IEEE Int. Geosci. Remote Sens. Symp.,* **3,** 1675–1677.
——, E. E. Clothiaux, G. G. Mace, S. Kato, and X. Dong, 2001: Retrieval of cloud liquid water path using microwave radiometer measurements. *J. Geophys. Res.,* **106,** 14 485–14 500.
Lovejoy, S., M. R. Duncan, and D. Schertzer, 1996: Scalar multifractal radar observer's problem. *J. Geophys. Res.,* **101,** 26 479–26 491.
Marshak, A., A. Davis, W. Wiscombe, and R. Cahalan, 1997: Scale invariance in liquid water distributions in marine stratocumulus. Part II: Multifractal properties and intermittency issues. *J. Atmos. Sci.,* **54,** 1423–1444.
McFarlane, S. A., K. F. Evans, E. J. Mlawer, and E. E. Clothiaux, 2000: Shortwave flux closure experiments at Nauru. *Proc. 10th ARM Science Team Meeting,* San Antonio, TX, U.S. Dept. of Energy, 1–7.
Monin, A. S., and A. M. Yaglom, 1975: *Statistical Fluid Mechanics.* Vol. 2. MIT Press, 683 pp.
Panter, P. F., 1965: *Modulation, Noise, and Spectral Analysis.* McGraw-Hill, 759 pp.
Pelletier, J. D., 1997: Kardar-Parisi-Zhang scaling of the height of the convective boundary layer and fractal structure of cumulus cloud fields. *Phys. Rev. Lett.,* **78,** 2672–2675.
Peng, C.-K., S. V. Buldyrev, A. L. Goldberger, S. Havlin, F. Sciortino, M. Simmons, and H.-E. Stanley, 1992: Long-range correlations in nucleotide sequences. *Nature,* **356,** 168–170.
——, ——, S. Havlin, M. Simmons, H.-E. Stanley, and A. L. Goldberger, 1994: On the mosaic organization of DNA sequences. *Phys. Rev. E,* **49,** 1685–1689.
Percival, D. B., and A. T. Walden, 1994: *Spectral Analysis for Physical Applications: Multitaper and Conventional Univariate Techniques.* Cambridge University Press, 583 pp.
Priestley, M. B., 1981: *Spectral Analysis and Time Series.* Academic Press, 890 pp.
Schroeder, J. A., and E. R. Westwater, 1991: User's guide to WPL microwave radiative transfer software. NOAA Tech. Memo. ERL WPL-213, 37 pp.
Schroeder, M., 1991: *Fractals, Chaos, Power Laws.* W. H. Freeman and Co., 429 pp.
Stanley, H. E., S. V. Buldyrev, A. L. Goldberger, S. Havlin, C.-K. Peng, and M. Simons, 1993: Long-range power-law correlations in condensed matter physics and biophysics. *Physica A,* **200,** 4–24.
Stokes, G. M., and S. E. Schwartz, 1994: The Atmospheric Radiation Measurement (ARM) program: Programmatic background and design of the cloud and radiation test bed. *Bull. Amer. Meteor. Soc.,* **75,** 1201–1221.
Vandewalle, N., and M. Ausloos, 1997: Coherent and random sequences in financial fluctuations. *Physica A,* **246,** 454–459.
——, and ——, 1998: Extended detrended fluctuation analysis for financial data. *Int. J. Comput. Anticipat. Syst.,* **1,** 342–349.
Tessier, Y., S. Lovejoy, and D. Schertzer, 1993: Universal multifractals: Theory and observations for rain and clouds. *J. Appl. Meteor.,* **32,** 223–250.
Turcotte, D. L., 1997: *Fractals and Chaos in Geology and Geophysics.* Cambridge University Press, 398 pp.
Westwater, E. R., 1978: The accuracy of water vapor and cloud liquid water determination by dual-frequency ground-based microwave radiometry. *Radio Sci.,* **13,** 677–685.
——, 1993: Ground-based microwave remote sensing of meteorological variables. *Atmospheric Remote Sensing by Microwave Radiometry.* M. A. Janssen, Ed., John Wiley and Sons, 145–213.